# The Cook's Instability: Coiling of a Thread of Honey

**N. M. Ribe**[1], **M. Habibi**[2,3] **& Daniel Bonn**[3,4]

1. *Dynamique des Fluides Géologiques, IPGP et Université de Paris-7, CNRS*
*Tour 14, 2, place Jussieu, 75005 Paris, France*
*ribe@ipgp.jussieu.fr*

2. *Institute For Advanced Studies in Basic Sciences, Zanjan 45195-1159, Iran*

3. *Laboratoire de Physique Statistique, UMR 8550 CNRS, École Normale Supérieure,*
*24, rue Lhomond, 75231 Paris Cedex 05, France*

4. *Van der Waals-Zeeman Institute, University of Amsterdam,*
*Valckenierstraat 65, 1018 XE Amsterdam, the Netherlands*

## Abstract :

*We combine analytical, numerical, and experimental approaches to study the dynamics of the 'liquid rope coiling' that occurs when a thin stream of viscous fluid like honey falls onto a surface. As the fall height increases, coiling traverses a sequence of four dynamical regimes (viscous, gravitational, inertio-gravitational, and inertial) characterized by different balances of the forces acting on the rope. The inertio-gravitational regime is particularly rich, exhibiting multiple states that correspond to resonant modes of the rope's 'tail'.*

## Résumé :

*Nous étudions avec des méthodes analytique, numérique et expérimentale le flambage hélicoïdal d'un mince filet de fluide visqueux (e.g., miel) qui tombe sur une surface. Lorsque la hauteur de chute augmente, quatre régimes de l'instabilité se succèdent (visqueux, gravitationnel, inertio-gravitationnel, inertiel) qui correspondent aux différents équilibres de forces dans le filet. Le régime inertio-gravitationnel s'avère particulièrement riche, avec des états multiples qui représentent des modes resonants dans la "queue" du filet.*

## Key-words :

**liquid rope coiling; buckling instabilities**

## 1 Introduction

A thin stream of honey falling onto a piece of toast winds itself into a whirling "corkscrew". This instability was called "liquid rope coiling" by Barnes & Woodcock (1958), who were the first to study it experimentally. In these and in most later experiments, fluid with density $\rho$, viscosity $\nu$ and surface tension coefficient $\gamma$ is ejected at a volumetric rate $Q$ from a hole of diameter $d \equiv 2a_0$ and then falls a distance $H$ onto a solid surface (fig. 1.)

Among the milestones of the nearly 50 years of work on liquid rope coiling is the recognition by Taylor (1969) that the phenomenon is a buckling instability that requires a longitudinal compressive stress. Tchavdarov *et al.* (1993) performed a linear stability analysis of a stagnating viscous jet to determine the fall height and frequency at the onset of coiling. Mahadevan *et al.* (2000) demonstrated that coiling in the high-frequency limit is governed by a balance between rotational inertia and viscous forces. Our own study of this problem during the past few years combines analytical, numerical, and experimental approaches to reveal a hitherto unsuspected complexity in this common instability.

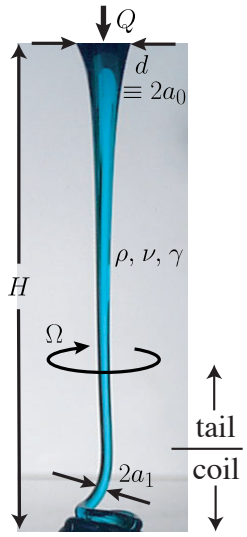


Figure 1: Steady coiling of a 'rope' of viscous corn syrup (photograph by N. Ribe.) Fluid with density $\rho$, viscosity $\nu$ and surface tension coefficient $\gamma$ is injected at volumetric rate $Q$ through a hole of diameter $d \equiv 2a_0$ and falls a distance $H$ onto a plate. The radius of the rope at its point of contact with the plate is $a_1$, and the angular coiling frequency is $\Omega$.

## 2 Experimental observations

Maleki *et al.* (2004), Ribe *et al.* (2006) and Habibi *et al.* (2006) used two different experimental setups to observe coiling over the widest possible range of fall heights and frequencies. In the first setup, designed for higher frequencies, the working fluid drained through a hole in the bottom of a reservoir maintained at constant head. The second setup, in which the working fluid is extruded at a constant rate from a syringe pump driven by a stepper motor, permitted access to very low fall heights and frequencies. Fig. 2 shows the measured frequency $\Omega$ as a function of fall height $H$ for three different experiments. A wide variety of behavior is observed. In fig. 2a, the frequency first decreases strongly with height and then slowly increases. In fig. 2b, the frequency is a strongly increasing function of height, but there is a gap at $H \approx 7$ cm where no coiling states were observed. Finally, in fig. 2c two or three distinct coiling states with different frequencies can be observed at a fixed height within a certain range.

## 3 Numerical model

To make sense of the variety of behavior shown in fig. 2, Ribe (2004) constructed a numerical model based on an asymptotic theory that describes the arbitrary time-dependent motion of a slender rope of viscous fluid. Motion of the rope is driven by buoyancy and by the imposed volumetric ejection rate $Q$, and resisted by viscous forces and inertia. Surface tension forces are also included, but typically have only a small (few percent) effect on the coiling frequency.

Because the motion of the rope is steady in the corotating reference frame, all the variables describing its motion are functions only of the arclength $s$ along the rope's axis, where $s = 0$ at the ejection hole and $s = \ell$ (say) at the rope's point of contact with the surface. The equations describing the rope's geometry, kinematics, and dynamics (force and torque balance) constitute a seventeenth-order system of ODEs in the independent variable $s$. Because the coiling frequency $\Omega$ and the rope length $\ell$ are unknown, nineteen boundary conditions at the ends $s = 0$ and $s = \ell$ are required. The resulting seventeenth-order two-point boundary-value problem is solved using a numerical continuation method.

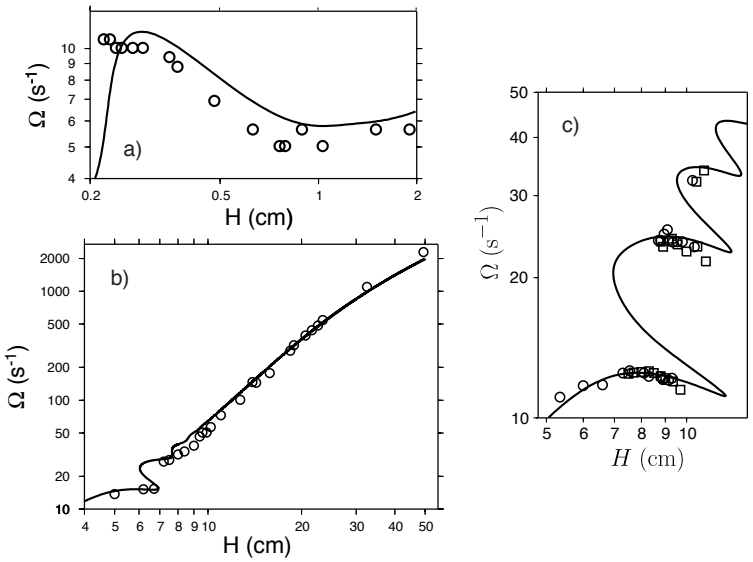


Figure 2: Coiling frequency vs. fall height measured experimentally (symbols) and calculated numerically (solid lines) for silicone oil ($\rho = 0.97$ g cm$^{-3}$, $\gamma = 21.5$ dyne cm$^{-1}$) and three sets of values of $\{\nu, d, Q\}$ in units of $\{\mathrm{cm}^2\mathrm{s}^{-1}$, cm, $\mathrm{cm}^3\mathrm{s}^{-1}\}$: (a) $\{1000, 0.068, 0.0038\}$; (b) $\{300, 0.5, 0.094\}$; (c) $\{1000, 0.068, 0.00215\}$.

The solid line in each panel of fig. 2 shows the coiling frequency predicted by the numerical model for the same values of $\nu$, $\rho$, $\gamma$, $d$ and $Q$ as in the corresponding laboratory experiment. The agreement with the experimental measurements, with no free parameters, is very good overall. Our next task is to interpret its physical significance.

## 4 Regimes of liquid rope coiling

Consider now the 'coil' portion of the rope (fig. 1), where deformation occurs primarily by bending and twisting. The viscous forces that resist these deformations can be balanced in three ways. At very low fall heights for which gravity and inertia are both negligible, the viscous forces can only be balanced by other viscous forces, resulting in a zero net viscous force on every fluid element. At greater heights, the buoyancy force becomes sufficiently large to balance the viscous forces. Finally, at still greater heights the viscous forces are balanced primarily by inertia. Mahadevan *et al.* (2000) and Ribe (2004) showed that these balances imply the existence of three distinct coiling regimes - 'viscous" ($V$), 'gravitational' ($G$), and 'inertial' ($I$) - for which the coiling frequencies are proportional to the scales

$$\Omega_V = \frac{Q}{Ha_1^2}, \qquad \Omega_G = \left(\frac{gQ^3}{\nu a_1^8}\right)^{\frac{1}{4}}, \qquad \Omega_I = \left(\frac{Q^4}{\nu a_1^{10}}\right)^{\frac{1}{3}}. \tag{1}$$

To verify that these three regimes actually exist, Ribe (2004) and Maleki *et al.* (2004) rescaled their numerical and experimental results, respectively, in a way that reveals clearly the transitions between pairs of regimes. For the transition from the $G$ to the $I$ regime, for example, one plots the scaled frequency $\Omega/\Omega_G$ against $\Omega_I/\Omega_G$; the $G$ and $I$ regimes (if they exist) will then be represented by segments of the curve with slopes of zero and unity, respectively. These segments are clearly present on the left and right sides, respectively, of fig. 3a (rescaled numerics) and fig. 3b (rescaled experimental measurements), demonstrating the existence of the $G$ and $I$ regimes.

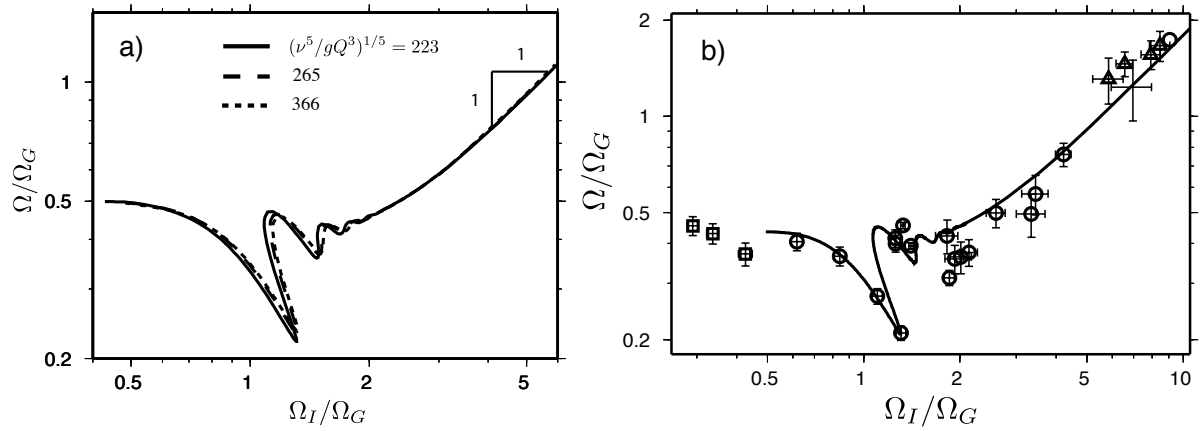


Figure 3: (a) Rescaled coiling frequency $\Omega/\Omega_G$ vs. $\Omega_I/\Omega_G$ for coiling in the gravitational (slope $= 0$) and inertial (slope $= 1$) regimes. (a) Numerical calculation for three values of the dimensionless viscosity $(\nu^5/gQ^3)^{1/5}$. (b) Experimental measurements (symbols) and numerical calculation (solid line) for silicone oil with $\nu = 300\ \mathrm{cm^2 s^{-1}}$, $d = 0.5$ cm, and $Q = 0.094\ \mathrm{cm^3 s^{-1}}$.

However, it is also clear from fig. 3 that something strange is going on between the $G$ and $I$ regimes, in the range $0.7 < \Omega_I/\Omega_G < 2$. This range corresponds to fall heights for which multiple coiling states with different frequencies can exist, as in fig. 2c. To understand the physical origin of these multiple states, we need to look more closely at the long and nearly vertical 'tail' portion of the rope (see fig. 1a.) The tail behaves as a 'viscous string' that deforms primarily by axial stretching induced by the pull of gravity, with negligible bending and twisting. Because the axis of the tail is slightly curved, the viscous force acting on the string has a small transverse component that is balanced by the buoyancy and centrifugal forces. Ribe *et al.* (2006) showed that in the limit of strong gravity-induced stretching, the amplitude $y(s)$ of the deflection of the string's axis from the vertical satisfies

$$\frac{gH}{\pi}\sin\frac{\pi(H-s)}{H}\frac{\mathrm{d}^2y}{\mathrm{d}s^2} - g\frac{\mathrm{d}y}{\mathrm{d}s} + \Omega^2 y = 0, \tag{2}$$

which has nontrivial solutions subject to the relevant boundary conditions only for particular values of the angular frequency $\Omega$. Each of these eigenvalues $\Omega_n$ is proportional to the simple pendulum frequency $(g/H)^{1/2} \equiv \Omega_{IG}$, where the subscript $IG$ ('inertio-gravitational') emphasizes that the modes in question involve both gravity and inertia and are observed at fall heights intermediate between those of the $G$ and the $I$ regimes. To test the simple viscous string model (2) against solutions of the complete seventeenth-order boundary-value problem for a coiling rope, Ribe *et al.* (2006) plotted the rescaled coiling frequency $\Omega/\Omega_{IG}$ vs. $\Omega_G/\Omega_{IG}$. On such a diagram (fig. 4) the multiple frequencies predicted by the full model appear as right-facing horizontal 'spikes' that coincide almost perfectly with the (numerically determined) eigenfrequencies $\Omega_n$ (horizontal black bars.) Physically speaking, the eigenfrequencies $\Omega_n$ correspond to resonant oscillations of the tail of the rope in response to forcing by the coil at the gravitational frequency $\Omega_G$. Three such resonant modes are evident in the experimental measurements shown in fig. 2c, and a fourth mode has been observed by Habibi *et al.* (2006). Ribe *et al.* (2006) and Habibi *et al.* (2006) showed that transitions between the modes occur in an apparently chaotic way, usually (but not always) with a change in the sense of the rotation of the coiling via an intermediate 'figure of eight' state.

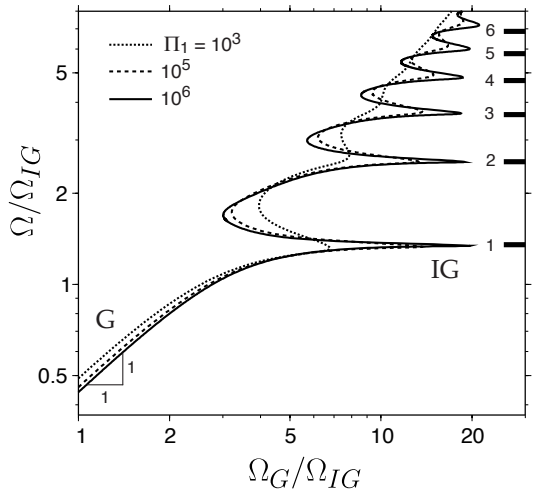


Figure 4: Rescaled frequency $\Omega/\Omega_{IG}$ vs. $\Omega_G/\Omega_{IG}$ in the limit of strong stretching ($a_1 \ll a_0$) calculated numerically for three values of the dimensionless viscosity $\Pi_1 = (\nu^5/gQ^3)^{1/5}$. Segments of the curves representing gravitational and inertio-gravitational coiling are denoted by $G$ and $IG$, respectively. The horizontal black bars (right) indicate the first six eigenfrequencies of a whirling viscous string described by (2).

## 5 Summary

All the results discussed above can be conveniently summarized in the form of a curve of coiling frequency vs. height for a large value of the dimensionless viscosity $\Pi_1 = (\nu^5/gQ^3)^{1/5}$. Fig. 5 shows the numerically calculated curve of dimensionless frequency $\Omega(\nu/g^2)^{1/3} \equiv \hat{\Omega}$ vs. dimensionless fall height $H(g/\nu^2)^{1/3} \equiv \hat{H}$ for $\Pi_1 = 7140$. For small heights $\hat{H} < 0.07$, coiling occurs in the viscous ($V$) regime, and the frequency decreases with height. The frequency then increases in the range $0.1 < \hat{H} < 0.4$, corresponding to the gravitational ($G$) regime. The inertio-gravitational regime appears next ($0.5 < \hat{H} < 1.1$), with multiple coiling states at a fixed fall height corresponding to the resonant 'viscous string' modes discussed above. Ribe *et al.* (2006) carried out a formal linear stability analysis of this regime which showed that the dashed portions of the curve in fig. 5 are unstable to small perturbations, in agreement with the fact that steady coiling states are never observed along these portions of the curve in the laboratory (see fig. 2c.) Finally, for $\hat{H} > 1.2$ the curve becomes smooth again as the inertial ($I$) regime takes over. Thus liquid rope coiling, so simple to realize in any home kitchen, turns out upon closer examination to exhibit surprisingly rich and complex behavior.

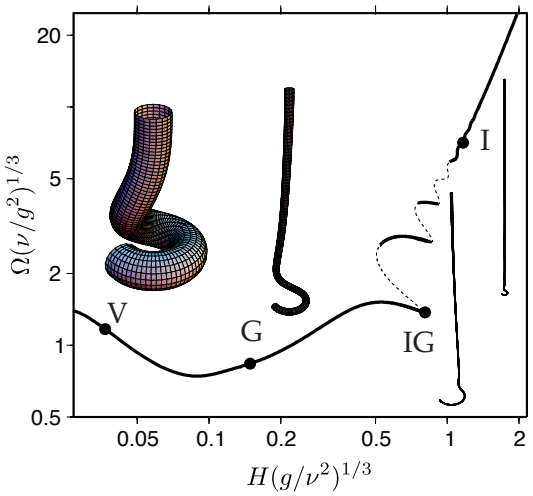


Figure 5: Steady coiling frequency calculated numerically as a function of height for $(\nu^5/gQ^3)^{1/5} = 7140$ and $(\nu Q/gd^4)^{1/4} = 3.67$. States located on the dashed portions of the curve are unstable to small perturbations. The inset images show the shape of the coiling rope at the four heights indicated by black dots, corresponding to the $V$, $G$, $IG$, and $I$ regimes.

## References

Barnes, G. & Woodcock, R. 1958 Liquid rope-coil effect. *Am. J. Physics* **26** 205-209

Habibi, M., Maleki, M., Golestanian, R., Ribe, N. M. & Bonn, D. 2006. Dynamics of liquid rope coiling. *Phys. Rev. E* **74** 066306

Mahadevan, L., Ryu, W. S. & Samuel, A. D. T. 2000. Correction: Fluid 'rope trick' investigated. *Nature* **403** 502

Maleki, M., Habibi, M., Golestanian, R., Ribe, N. M. & Bonn, D. 2004. Liquid rope coiling on a solid surface. *Phys. Rev. Lett.* **93** 214502

Ribe, N. M. 2004 Coiling of viscous jets. *Proc. R. Soc. Lond.* **A460** 3223-3239

Ribe, N. M., Huppert, H. E., Hallworth, M. A., Habibi, M. & Bonn, D. 2006 Multiple coexisting states of liquid rope coiling. *J. Fluid. Mech.* **555** 275-297

Ribe, N. M., Habibi, M. & Bonn, D. 2006 Stability of liquid rope coiling. *Phys. Fluids* **18** 084102

Taylor, G. I. 1969 Instability of jets, threads, and sheets of viscous fluid. In *Proc. 12th Intl. Congr. Appl. Mech.*, pp. 382-388, Springer-Verlag, Berlin.

Tchavdarov, B., Yarin, A. L. & Radev, S. 1993 Buckling of thin liquid jets. *J. Fluid. Mech.* **253** 593-615